CP4O

CryoSat Plus for Oceans

ESA/ESRIN Contract No. 4000106169/12/I-NB

WP3000 – Improved Estimation of the Thermal Noise in the SAMOSA Retracker

VERSION 3.1, March 31, 2016

ESA/ESRIN Technical Officer: Jérôme Benveniste

Starlab Barcelona S.L.
C/ TeodorRoviralta 45
08022 Barcelona, Spain
http://starlab.es

EUROPEAN SPACE AGENCY (ESA) CONTRACT REPORT
The work described in this report was done under ESA contract.
Responsibility for the contents resides in the author or organisation that prepared it.

AUTHOR/MANAGER/COLLABORATOR LIST

Main Author(s)	**Affiliation**	**Signature**
F. Martín	Starlab	
Project Manager	**Affiliation**	
A. Repucci	Starlab	
Collaborators	**Affiliation**	

DISTRIBUTION LIST

Who	**Affiliation**
Jérôme Benveniste, Américo Ambrosio, Marco Restano	ESA
David Cotton, Marcello Passaro	SatOC
Ole Andersen, Lars Stenseng	DTU Space
Mónica Roca, Pablo Nilo Garcia	IsardSAT
Paolo Cipollini	NOC
Mathilde Cancet	Noveltis

CHANGE RECORD

ISSUE	DATE	Change Record Notes	Main Author
1.0	14-12-2016	First Draft	F. Martín
2.0	13-02-2016	Updated Version	F. Martín
3.0	17-03-2016	Updated Version	F. Martín
3.1	31-03-2016	Updated Version	F. Martin

ACKNOWLEDGMENTS

This extension to the CP4O project has been funded by ESA under the Support to Science Element (STSE) programme

We wish to acknowledge the support of CNES and CLS who kindly provided the CNES-CPP data used in this work. CNES-CPP products were developed by CNES and CLS in the frame of the “Sentinel-3 SRAL SAR mode performance assessment” study.

Contents

Table of Figures

1 Introduction

The “CryoSat Plus for Oceans” (CP40) project is funded under the ESA Support To Science Elements Programme (STSE) and brings together an expert consortium comprising, CLS, isardSAT, NOC, Noveltis, SatOC, Starlab, TU Delft, and the University of Porto. The main objectives of CP40 are to:

- Build a sound scientific basis for new scientific and operational applications of CryoSat-2 data.
- Generate and evaluate new methods and products that will enable the full exploitation of the capabilities of the CryoSat-2 SIRAL altimeter.
- Ensure, that the scientific return of the CryoSat-2 mission is maximized.

Under the CCN some additional activities were supported to address some priority issues, including further optimisation of the SAMOSA retracker.

1.1 Purpose, Scope and Goals

The objective of the WP3000 of the CCN01 D.3.1 is to provide an optimized method for the estimation of the thermal noise on the SAR waveforms, that will be implemented in the operational SAMOSA retracker. Thermal noise is a key parameter in the retracking of the SAR waveforms, which is directly related to the estimation of the SWH (Significant Wave Height).

Within the framework of the original CP40 contract, an initial estimation and inclusion of the thermal noise on the SAMOSA was conducted by Starlab. In this work an empirical method was proposed, measuring the noise level directly in the SAR waveform considering the range gates located before the leading edge, and their position variability. However, preliminary results showed that the method needed to be optimized.

In this report on the work carried out under the CCN, the main features of the optimized SAMOSA retracker are detailed. Additionally an extensive data set has been used to evaluate the performance of the optimized retracker.

2 Background

The estimation of the thermal noise is a key parameter in the retracking of the SAR waveforms, since it affects directly the estimation of the SWH. Originally the noise level was obtained as the average value of the first SAR waveforms lags, typically lags 11-21. However, this approach does not consider the impact that the SWH can have both on the leading edge and on the amplitude of the averaged SAR waveform. Figure 1 serves as an example of this, where the SWH and peak waveform evolution from CryoSat-2 SAR mode data have been plotted, for two different days, showing different SWH conditions. As can be seen, the peak waveform evolution shows the same trend as the SWH.

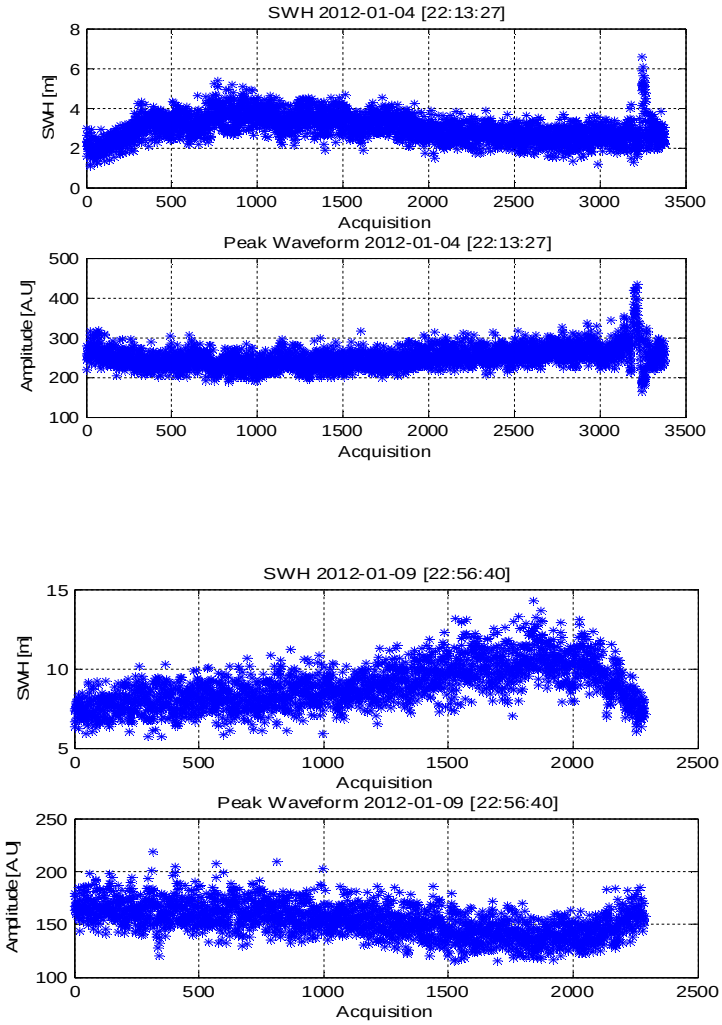

Figure 1- CryoSat-2 SWH and Amplitude Peak waveform evolution (Arbitrary Units).

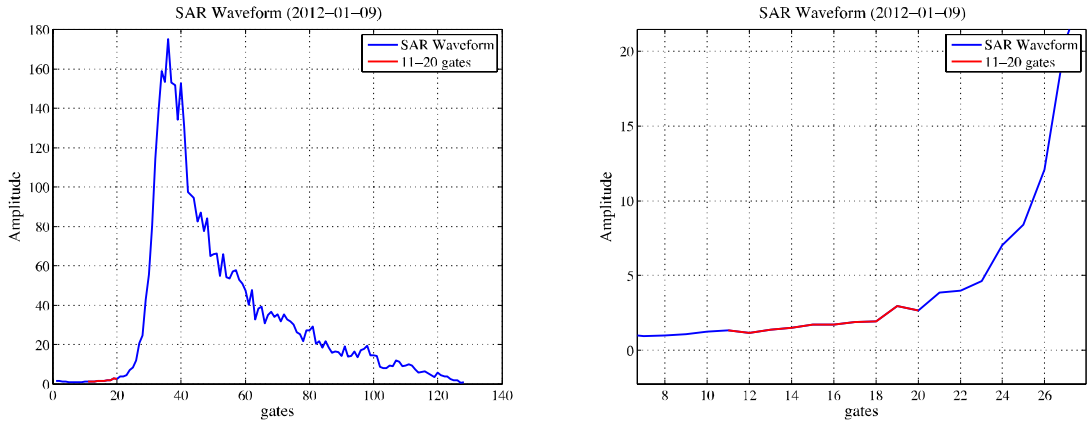

Figure 2- CryoSat-2 SAR waveform acquired on 2012-01-09.

Figure 2 shows a CryoSat-2 SAR waveform acquired on 2012-01-09. In this case gates 11-20 include part of the leading edge, thus not representing the true noise. Figure 3 shows CryoSat-2 SAR waveforms acquired on 2012-01-09, for two values of SWH (2.47m, and 6.59m). From this figure, a clear dependence of both the leading edge and the peak of the two waveforms, with respect to the SWH, can be appreciated over an interval of ~10 lags.

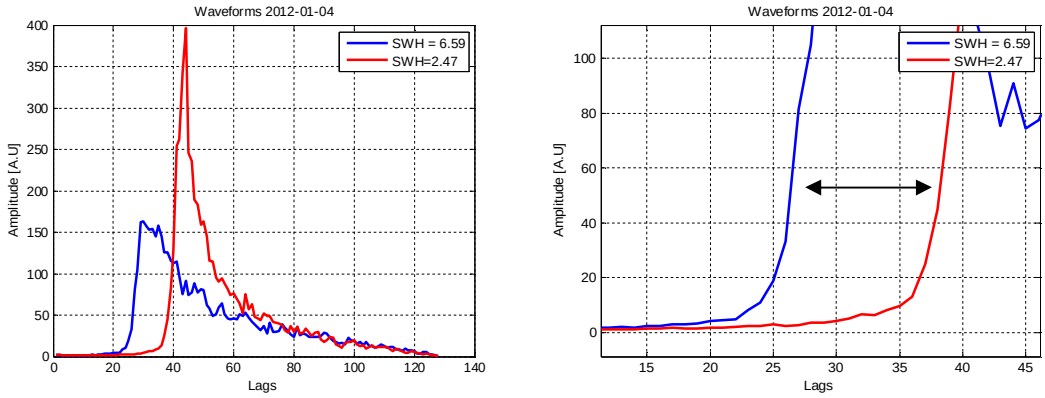

Figure 3- CryoSat-2 SAR waveforms acquired on 2012-01-02

These results suggest that the range position of the first gates of the leading edge can vary. In fact, depending on the SWH, the range position of the first gates of the leading edge can vary across 5 or more gates (Figure 3). Thus, using the noise floor averaged across a fixed range of lags (between 11 and 21), can lead to an erroneous noise floor estimation.

Therefore SWH should be considered in the estimation of the noise. Hence, in the framework of the CP40 project, an empirical model was proposed for the computation of the thermal noise. This approach was aimed at estimating the beginning of the leading edge,

subtracting two times the distance between the peak of the waveform and the half-peak point of the waveform. After that, an extra margin of 9 lags was added, in order to ensure that the leading edge was not considered as a noise region. Figure 4 shows how the noise floor is estimated.

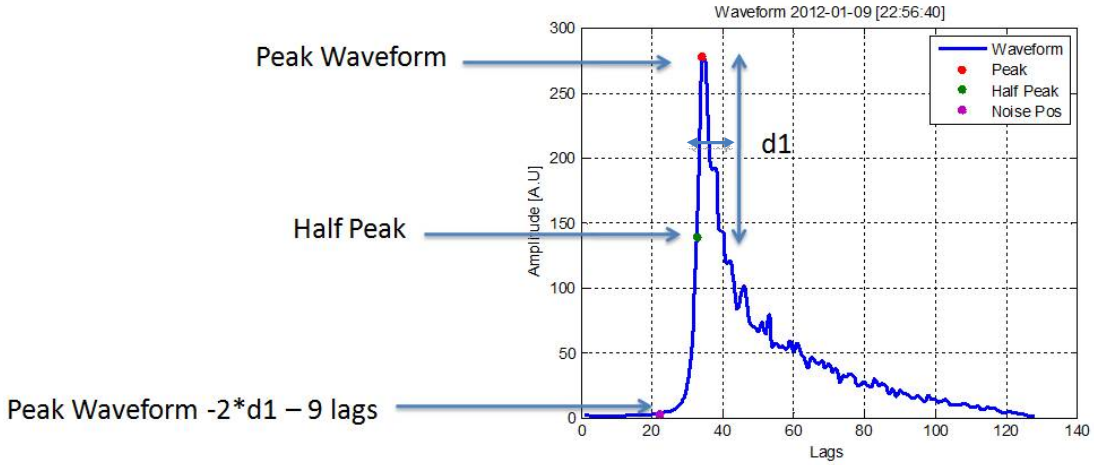

Figure 4- Empirical approach for estimate the waveform noise floor (note that d1 accounts for a segment on the horizontal axis whose extremes are referred to the lags related to the peak and to the half peak of the waveform).

However, does the fixed margin of 9 lags provide the optimum point for noise estimation for all cases? Figure 4 suggests that the definition of this margin needs to be optimized, as in some cases part of the leading edge could be erroneously included.

3 Optimisation of the Noise Floor Calculation

In the previous section it was shown that the range position of the first gate of the leading edge, depending on the SWH, can vary considerably. Therefore, the "fixed-lags" (11-21) approach can lead to an erroneous noise floor estimation. We describe below an optimization of this initial empirical approach.

In order to properly define the margin to the midpoint of the waveform leading edge (initially set equal to 9), an approach based on the uncorrelated characteristics of the thermal noise has been used. This technique exploits the nature of thermal noise, that is fully uncorrelated, and improves the SNR by averaging N independent SAR waveforms. Consequently, an SNR improvement by a factor $\sqrt{N}$ is obtained in the region where thermal noise dominates. To underline this improvement, the SNR has been computed for two representative data sets with different SWH characteristics (low and high SWH).

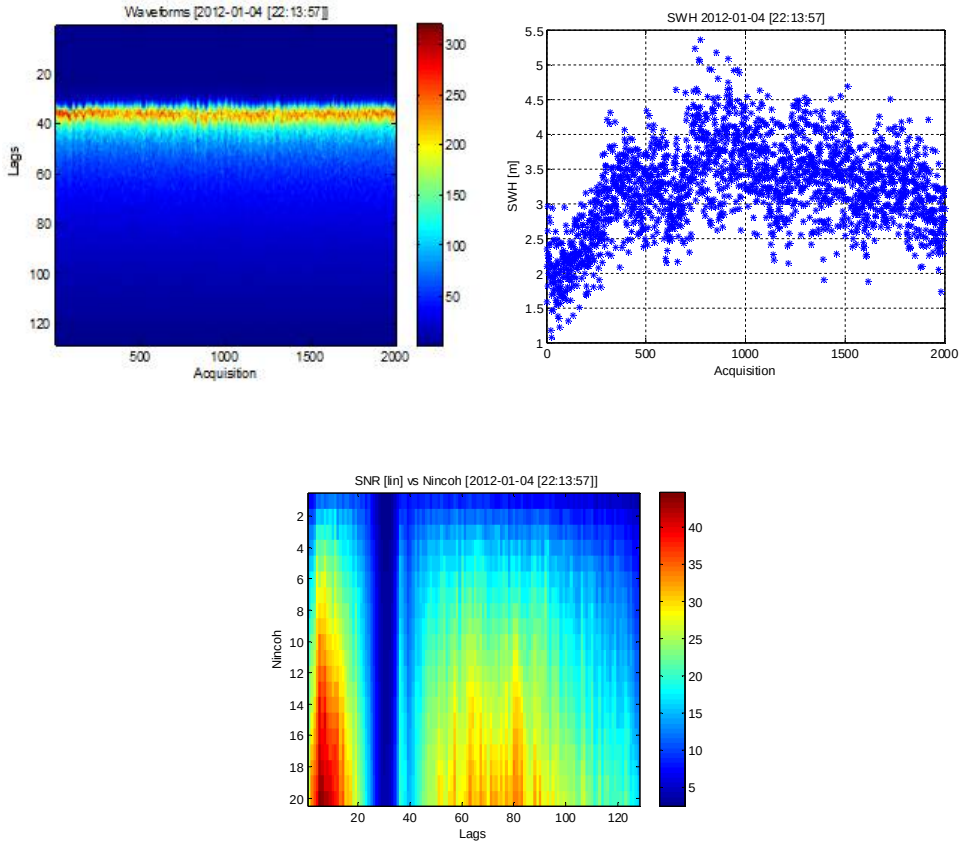

Figure 5- Waveforms (top left panel), SWH evolution (top right panel), and SNR (bottom panel) in linear units computed as a function of the number of independent waveforms (Nincoh) acquired on 2012-01-04 at 22:13:57.

Figure 5 show the SWH evolution for these data sets, the waveforms, and the SNR (in linear units) computed as a function of the number of independent waveforms (N_{incoh}). These plots reveal interesting issues. Firstly, the SNR tends to increase proportionally with $\sqrt{N_{incoh}}$ in the lags where the signal is uncorrelated (i.e. where thermal noise is present). At the same time, the leading edge position depends on the SWH, i.e. it tends to be shifted to the left side as the SWH increases (Figure 3). Additionally it can be observed that also the length of the noise floor depends on the SWH, being narrower for the higher SWHs (Figure 5, bottom panel 'SNR'). Thus, the new analysis shall determine the optimum position of the noise region, and in addition the optimum width (or number of lags) that shall be considered in the analysis.

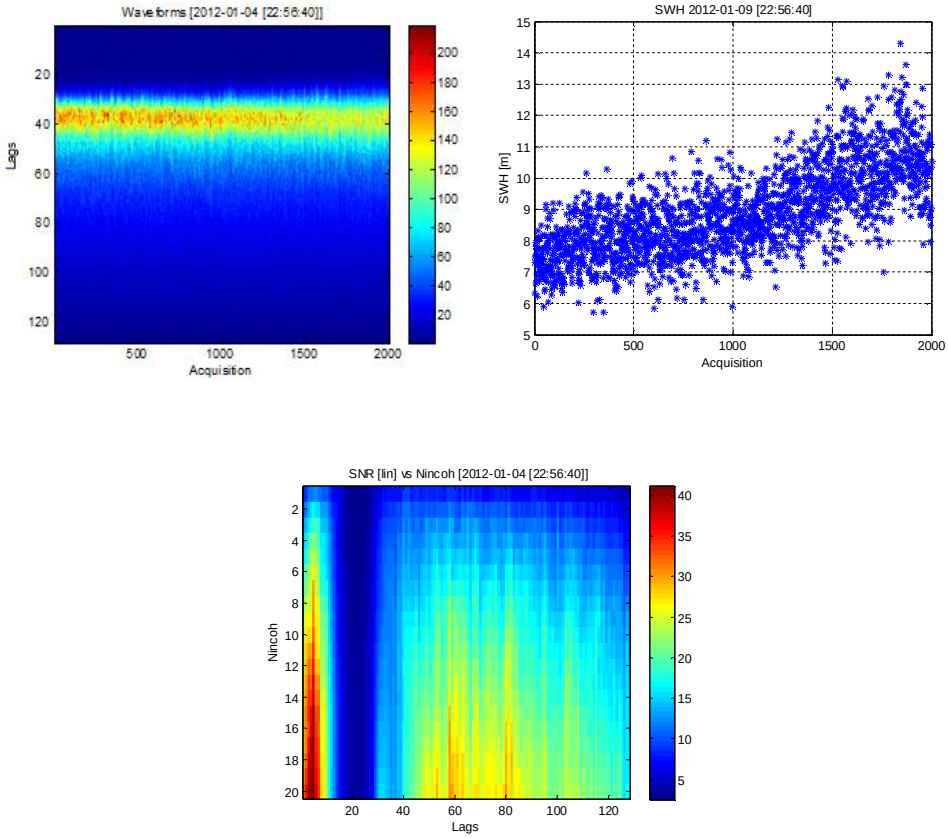

Figure 6- Waveforms (top left panel), SWH evolution (top right panel), and SNR (bottom panel) in linear units computed as a function of the number of independent waveforms (Nincoh) acquired on 2012-01-04 at 22:58:40.

Therefore, according to Figures 5-6, an initial margin of 14-16 lags and a width length of 2 lags represents a conservative choice for estimating the noise floor in different SWH conditions. Figure 7 shows which will be the optimum point for the noise floor for two different SWHs (low and high), considering a margin of 16 lags.

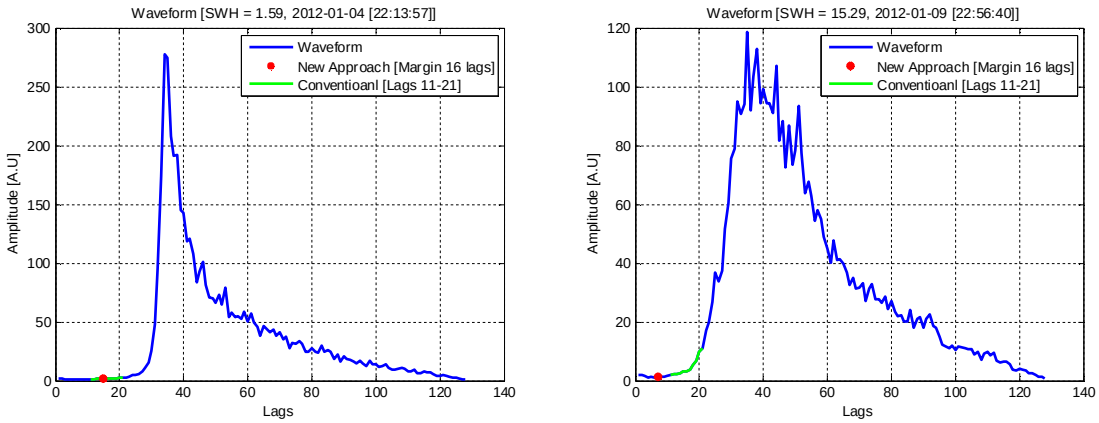

Figure 7- Optimum point for the noise floor estimation for two waveforms with SWH = 1.59m (left), and SWH=15.29m (right).

An initial validation was conducted for single tracks. The single tracks considered cover more than 20 latitude degrees and the SWH ranges between 2 and 4+ meters, which initially could be representative of general sea conditions. In Figure 8, as an example, the comparison between the SWH and SSH estimations provided by the SAMOSA re-tracker modified by Starlab (as decribed in this document), and the numerical re-tracker implemented in the CNES-CLS Cryosat Processing Prototype (CPP) data set is shown (See RD.10 for details of the CPP processor). The Starlab retracker is based on the SAMOSA-3 model, a further development of the previous SAMOSA models which now accounts for non-Gaussian ocean statistics, curvature effects in along and across-track, mispointing effects along and across-track, radial velocity effects, elliptical antenna pattern issues, and implements some of the basis functions using Look-Up Tables in order to improve the computation speed of the previous SAMOSA versions. The SAMOSA retracker algorithm is based on the use of LMS, which is a minimization process based on a Levenverg-Marquardt Algorithm. This process finds the best set of model parameters matching the data. Its main features can be found in [RD.8]. It can be seen that the differences between the SWH and SSH estimates from the updated thermal noise approach (“Starlab”) and the CPP solution are concentrated around zero with no significant slope along the whole track.

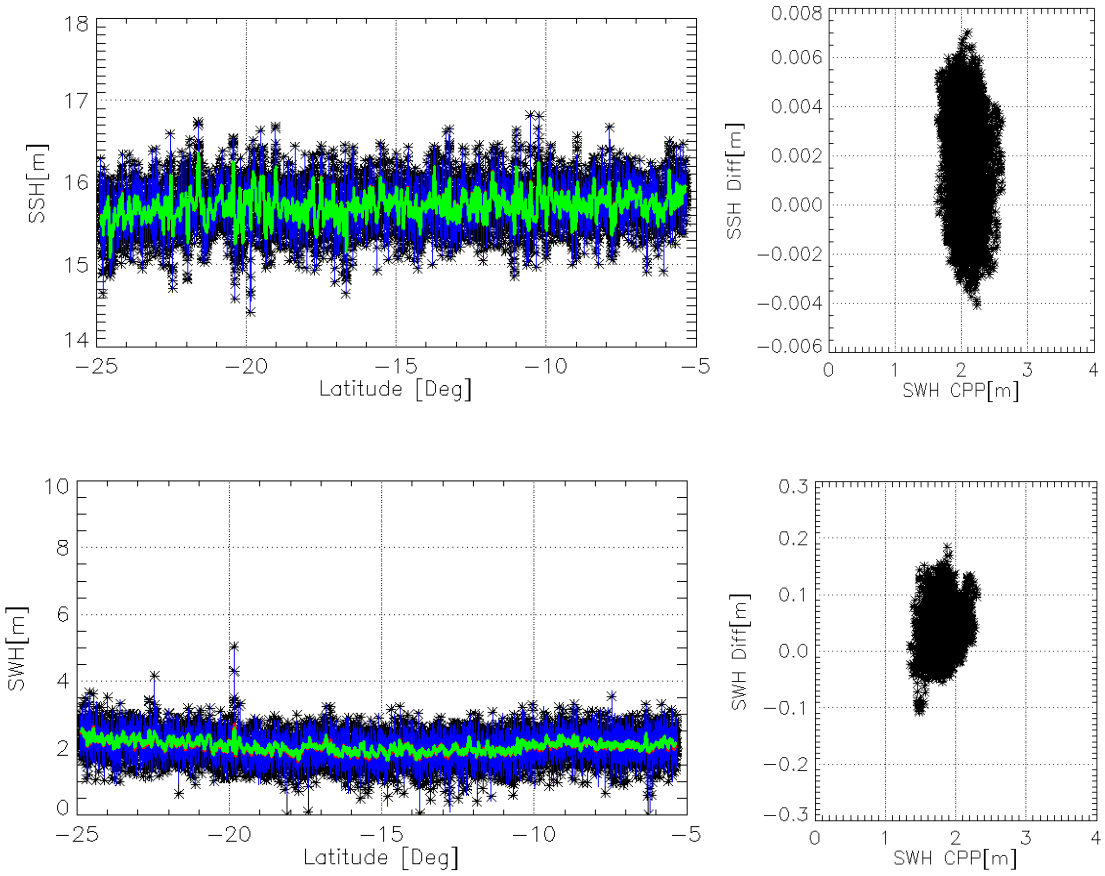

Figure 8- Difference between the Starlab SAMOSA and CPP retracking solutions: (upper left panel) SSH difference along the track (in dark blue SSH (Starlab), light blue SSH (CPP), red SSH after smoothing (Starlab), and green SSH after smoothing (CPP)); (upper right panel) SSH difference vs CPP SWH estimation; (bottom left panel) SWH difference along the track (in dark blue SWH (Starlab), light blue SWH (CPP), red SWH after smoothing (Starlab), and green SWH after smoothing (CPP)); (bottom right panel) SWH difference vs CPP SWH estimation

In order to provide a more robust validation, additional margins (i.e. 9, 14, 18) and different window lengths have been also investigated (Figures 9-12). Hence, an initial analysis was performed by using CryoSat-2 CNES-CPP L1b (v14) data collected during a month of operation (November 2012). This analysis allows a comparison of the retrieved Range (where Range is the distance from the satellite to the scattering point), Sea Surface Height (SSH), Significant Wave Height (SWH), and Power Units (Pu) for a wide range of different SWH conditions.

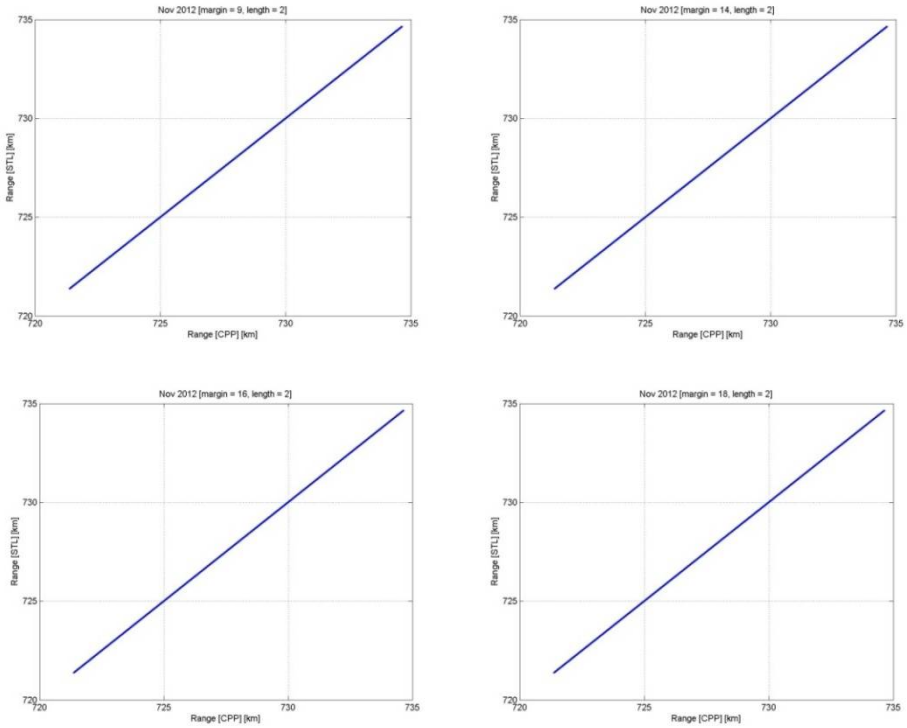

Figure 9- Scatter plot of range. CNES-CPP (x-axis) vs Starlab (y-axis). Margins of 9 (upper left panel), 14 (upper right panel), 16 (bottom left panel), and 18 (bottom right panel) lags.

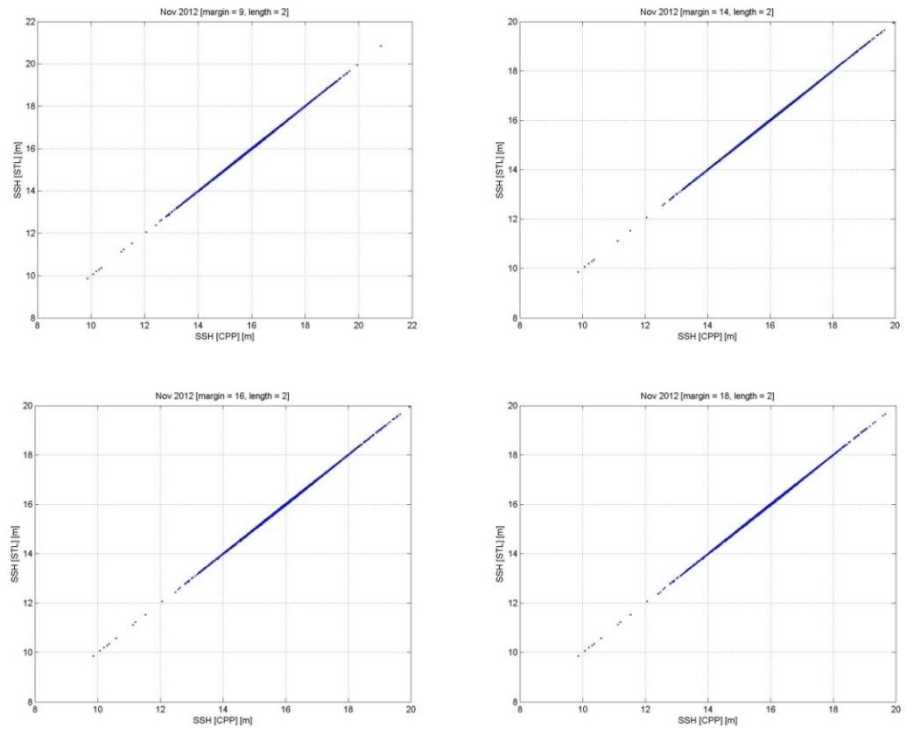

Figure 10- Scatter plot of SSH. CNES-CPP (x-axis) vs Starlab (y-axis). Margins of 9 (upper left panel), 14 (upper right panel), 16 (bottom left panel), and 18 (bottom right panel) lags.

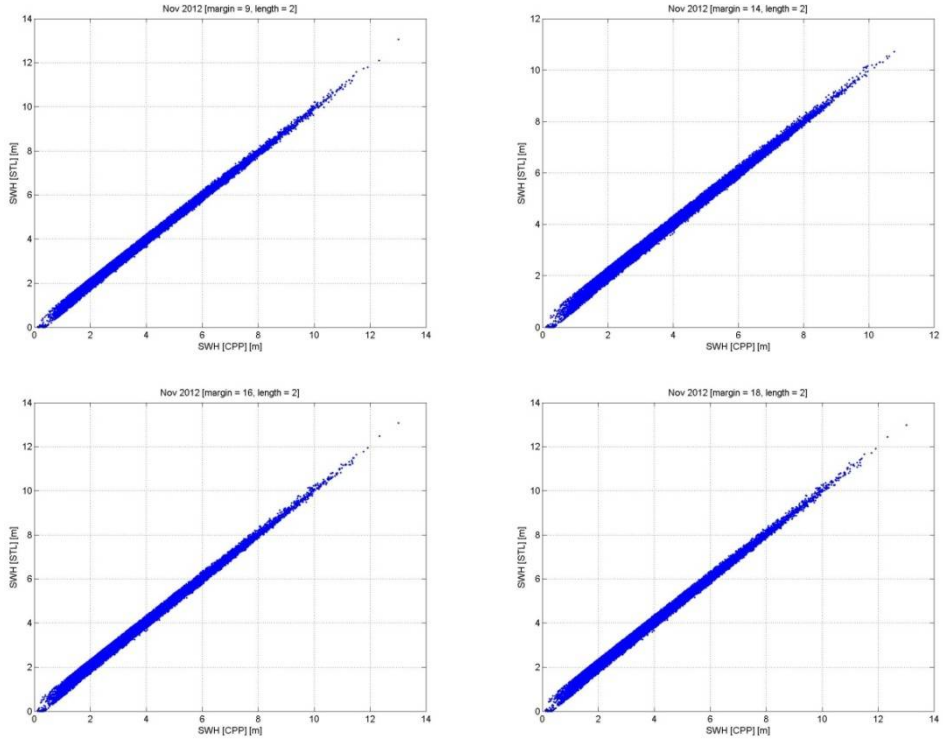

Figure 11- Scatter plot of SWH. CNES-CPP (x-axis) vs Starlab (y-axis). Margins of 9 (upper left panel), 14 (upper right panel), 16 (bottom left panel), and 18 (bottom right panel) lags.

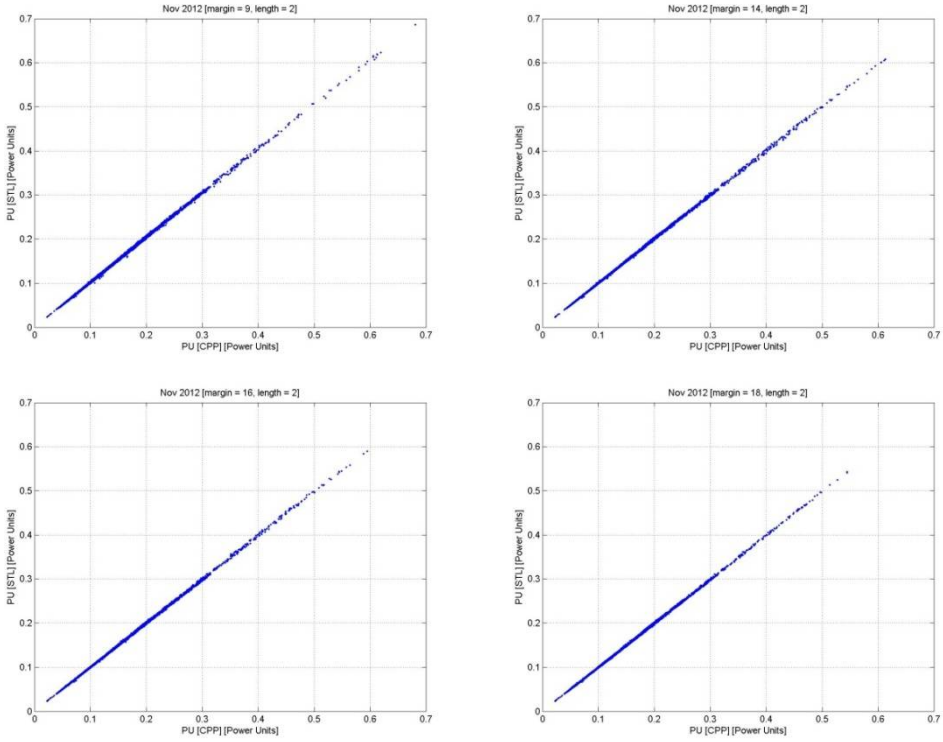

Figure 12- Scatter plot of Pu. CNES-CPP (x-axis) vs Starlab (y-axis). Margins of 9 (upper left panel), 14 (upper right panel), 16 (bottom left panel), and 18 (bottom right panel) lags.

Figure 9-12 plot the comparison between the range, SSH, SWH, and Pu, between the CNE-CPP and the SAMOSA retracker modified by Starlab for the different margins (i.e. 9, 14, 16, 18). As can be seen in general terms for the different parameters, there is a high correlation (higher than 99% for all the cases). The largest differences are seen in the SWH for the lower values, where the estimation provided by the Starlab SAMOSA retracker is a bit noisier.

In order to determine which margin is the optimum one, the errors (bias + the std of the error mean, and std) were computed for each case. Table 1 summarizes the error (bias and std) for SSH, SWH, and Pu for the different margins. From this, we see that a similar performance is obtained for the margins 9, 14, and 16 for the range and SSH estimation. For the Pu and SWH estimation, better performance in terms of error bias and standard deviation is achieved when the margins are 14 and 16. The worst results are obtained when the margin is set to 18 lags.

Table 1- Error bias, and std, obtained for the retrieved parameters, for different margins (9, 14, 16 and 18).

	SSH		**SWH**		**Pu**	
	Bias	**Std**	**Bias**	**Std**	**Bias**	**Std**
9	0.0047±1.63e-5$\left(\sim\frac{0.0054}{\sqrt{108715}}\right)$	0.0054	0.0795±2.64e-4$\left(\sim\frac{0.0872}{\sqrt{108715}}\right)$	0.0872	-0.0019±2.92e-6$\left(\sim\frac{9.71e-4}{\sqrt{108715}}\right)$	9.71e-4
14	**0.0055±1.63e-5**$\left(\sim\frac{0.0054}{\sqrt{108408}}\right)$	**0.0054**	**0.0092±2.96e-4**$\left(\sim\frac{0.0975}{\sqrt{108408}}\right)$	**0.0975**	**-2.78e-4±1.51e-6**$\left(\sim\frac{5.03e-4}{\sqrt{108408}}\right)$	**5.03e-4**
16	**0.0058±1.70e-5**$\left(\sim\frac{0.0058}{\sqrt{108844}}\right)$	**0.0058**	**-0.007±3.03e-4**$\left(\sim\frac{0.1}{\sqrt{108844}}\right)$	**0.1**	**8.30e-5±1.43e-6**$\left(\sim\frac{4.77e-4}{\sqrt{108844}}\right)$	**4.77e-4**
18	0.0059±1.77e-5$\left(\sim\frac{0.0058}{\sqrt{108747}}\right)$	0.0058	-0.0191±3.09e-4$\left(\sim\frac{0.1019}{\sqrt{108747}}\right)$	0.1019	3.54e-4±1.43e-6$\left(\sim\frac{4.75e-4}{\sqrt{108747}}\right)$	4.75e-4

In a following step the analysis has been repeated considering different window lengths. Table 2 summarizes the main results, showing no significant differences between them.

Table 2- Error bias, and std, obtained for the retrieved parameters, for different windows lengths (1, 2, 3, 4).

	SSH		SWH		Pu	
	Bias	**Std**	**Bias**	**Std**	**Bias**	**Std**
1	0.0058±1.75e-5$\left(\sim\frac{0.0058}{\sqrt{108844}}\right)$	0.0058	-0.0071±3.03e-4$\left(\sim\frac{0.1002}{\sqrt{108844}}\right)$	0.1002	8.572e-5±1.47e-6$\left(\sim\frac{4.908e-4}{\sqrt{108844}}\right)$	4.908e-4
2	**0.0058±1.75e-5**$\left(\sim\frac{0.0058}{\sqrt{108844}}\right)$	**0.0058**	**-0.0068±3.03e-4**$\left(\sim\frac{0.1}{\sqrt{108844}}\right)$	**0.1**	**7.8129-5±1.39e-6**$\left(\sim\frac{4.68e-4}{\sqrt{108844}}\right)$	**4.68e-4**
3	**0.0058±1.75e-5**$\left(\sim\frac{0.0058}{\sqrt{108852}}\right)$	**0.0058**	**-0.0068±3.03e-4**$\left(\sim\frac{0.1}{\sqrt{108852}}\right)$	**0.1**	**7.969e-5±1.41e-6**$\left(\sim\frac{4.7e-4}{\sqrt{108852}}\right)$	**4.7e-4**
4	0.0058±1.75e-5$\left(\sim\frac{0.0058}{\sqrt{108849}}\right)$	0.0058	-0.007±3.03e-4$\left(\sim\frac{0.1}{\sqrt{108849}}\right)$	0.1	8.30e-5±1.434-6$\left(\sim\frac{4.77e-4}{\sqrt{108849}}\right)$	4.77e-4

4 Validation Activities

The previous section described the empirical approach for the estimation of the noise floor. Additionally, an initial comparison was performed between results obtained from this approach and outputs of the SAR numerical retracker model developed by CNES, as provided in CPP Level-1b products, for different margins to the waveform leading edge (mid-point), and different window lengths applied in the Starlab implementation.

In this section the developed approach is validated using a one year data set from CryoSat-2 CNES-CPP L1b (v14).

4.1 Evaluation Data Set

Data from CryoSat-2 CNES-CPP L1b (v14) have been used as input to evaluate the different margins and window lengths for the thermal noise. The analysis was focused on the area where in situ data (wave buoy data) are available (30º-65ºN and 20º-0º W), and for the period 01/11/2012 – 31/12/2013. Figure 13 shows the area selected to perform the analysis (from Google Earth). The specification of the L2 data products generated by Starlab is given in APPENDIX A.

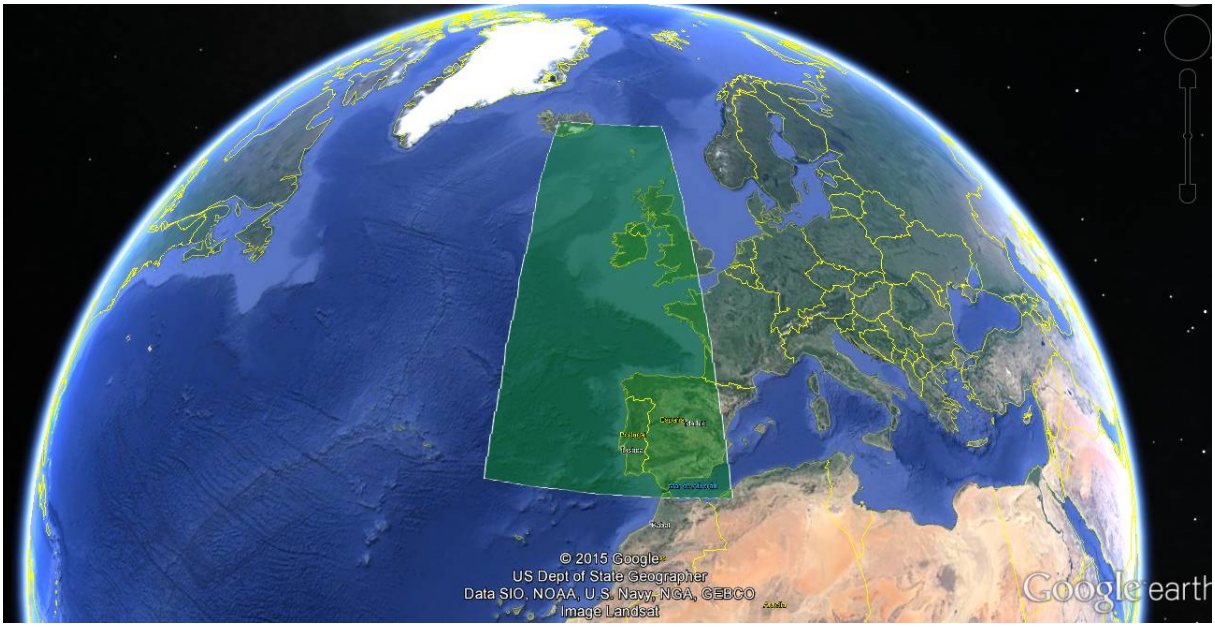

Figure 13- Area used to analyze the different approaches.

4.2 Wrong Data Removal

Wrong data were removed from the adopted dataset, filtering it as a function of the waveform amplitude. Therefore, a threshold has been defined, and files containing waveforms with amplitude higher than the threshold have been discarded. Based on the minimum amplitude of the waveforms contaminated (see APPENDIX B), the amplitude threshold has been set up to 10. Figure 14 shows an example of land contaminated waveform found on the data set analysed. Surprisingly, a large part of the data set included useless or contaminated products. Figure 15 plots all the points tracked during January 2013, “contaminated” data are coloured red, ”good” in blue. It is clear that there is a high percentage of the data that is not useful for the analysis (around 60% approx). Part of these data have been acquired over land, or close to the coast (land contamination). However, many of these “contaminated” data records have been acquired far away from the coast, so excluding the possibility of land contamination. A third reason to explain the distorted waveforms could be the presence of long swell waves.

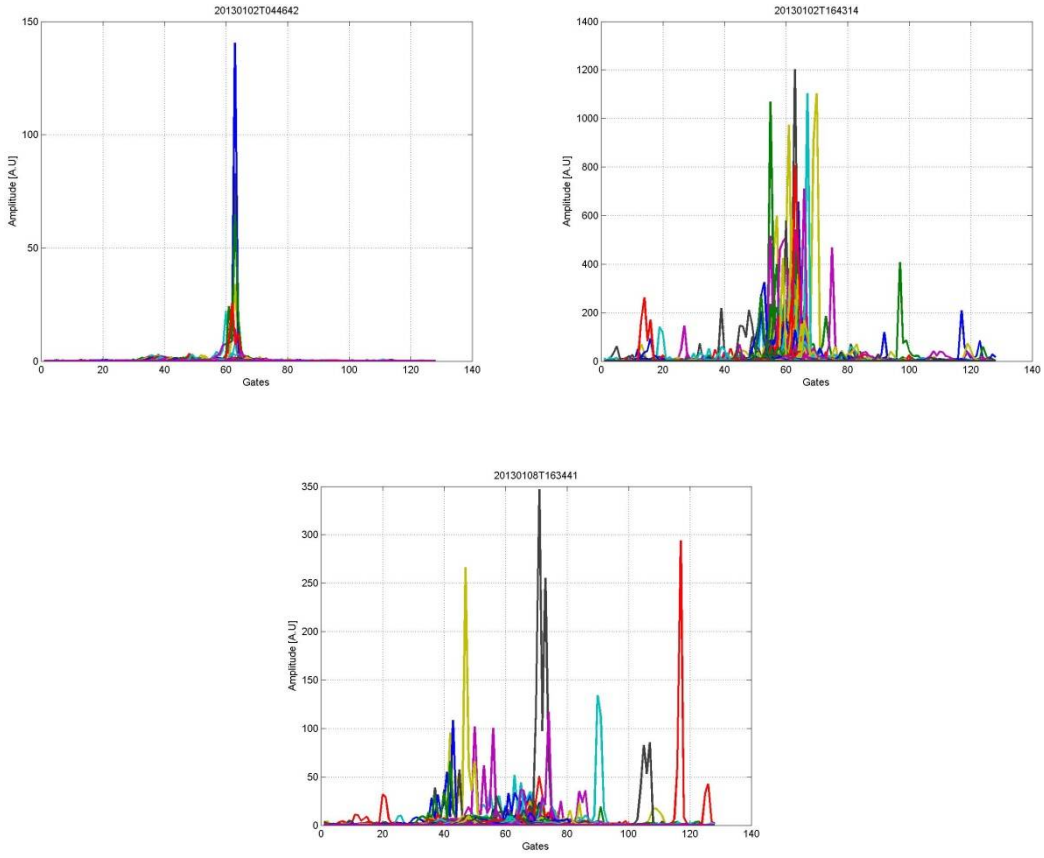

Figure 14- Example of Waveforms contaminated.

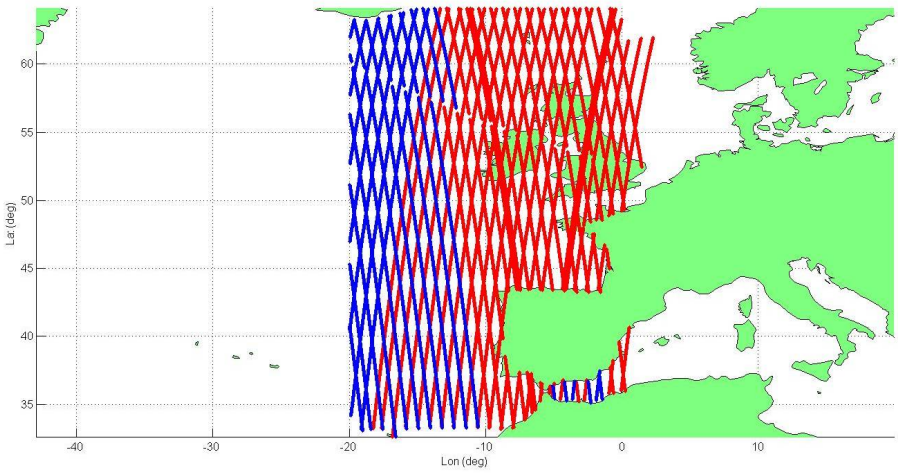

Figure 15- Area analysed, blue points correspond to good data, red points to "contaminated" data

4.3 Sea Surface Height Error Analysis

Figure 16 shows the comparison of the SSH obtained from Starlab and CNES-CPP retrackers. The scatter plot shows that both solutions are fully consistent, with no trend or bias observable.

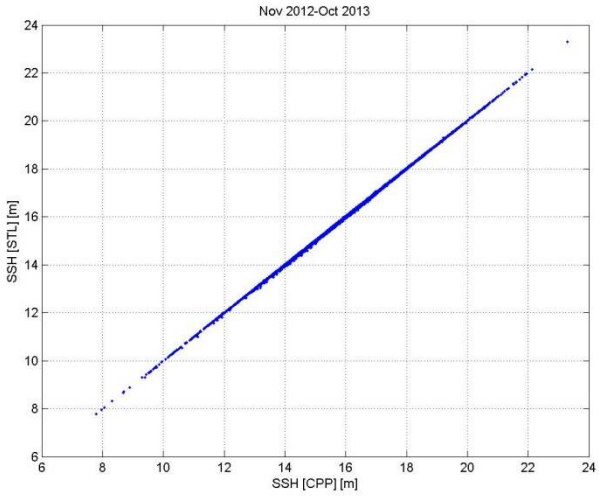

Figure 16- Scatter plot of SSH for CNES-CPP (x-axis), vs Starlab (y-axis).

Figure 17 shows the error i.e SSH starlab – SSH CNES-CPP, as a function of the CNES-CPP solutions (here considered as a reference). In general terms the density plots show the distributions around zero for the whole SSH. The 20 Hz error bias obtained is about 3 mm, with a standard deviation of 7 mm.

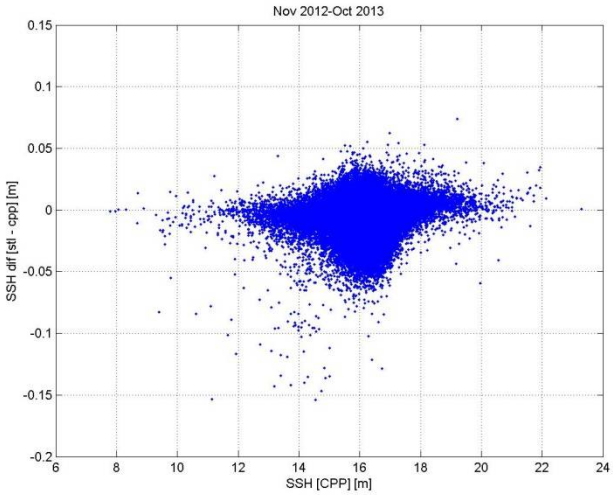

Figure 17- SSH error (SSH Starlab - SSH CNES-CPP) vs SSH CNES-CPP.

4.4 Significant Wave Height Error Analysis

A similar procedure has been employed to analyse the error in the SWH solutions. As can be seen in Figure 18, there is a high correlation (higher than 99% for all the cases). However, major SWH differences are obtained at low SWHs (Figure 19). The SWH error bias is -1.27 cm, the error standard deviation is about 20 cm.

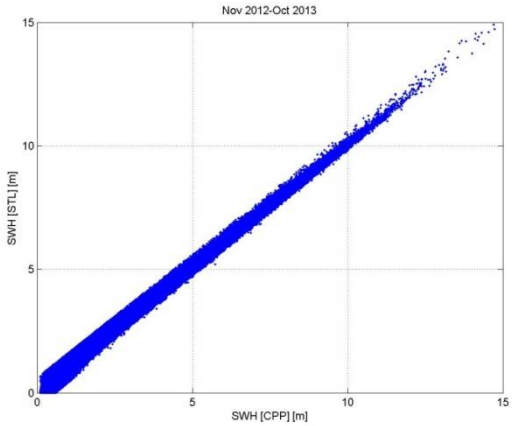

Figure 18- Scatter plot of SWH for CNES-CPP (x-axis), vs Starlab (y-axis).

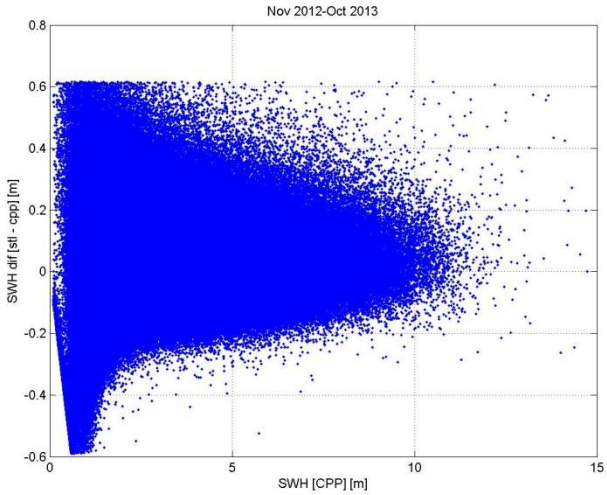

Figure 19- SWH error (SWH Starlab - SWH CNES-CPP) vs SWH CNES-CPP.

4.5 Waveform Power (Pu) Error Analysis

Now the waveform power (Pu) error is analysed. As can be seen in Figure 20, the Pu estimated by Starlab is perfectly aligned with the one estimated by CNES-CPP. In fact, Figure 21 shows that the differences are quite low. An error bias of 1.0479e-04, and an error standard deviation of 6.5914e-04 are obtained for the Pu.

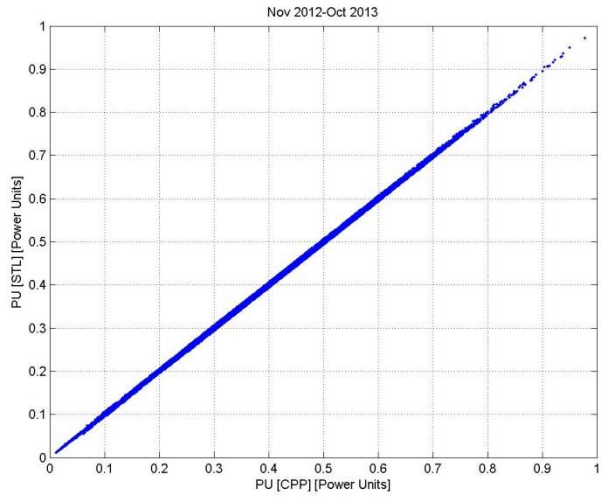

Figure 20- Scatter plot of Pu for CNES - CPP (x-axis), vs Starlab (y-axis).

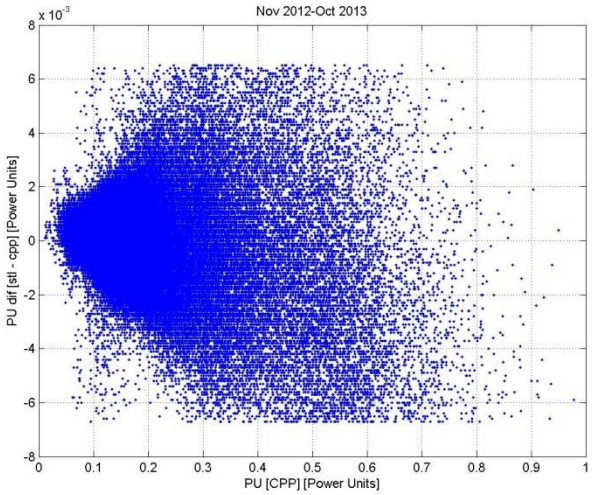

Figure 21- Pu error (Pu Starlab - Pu CNES-CPP) vs Pu CNES-CPP.

4.6 SSH and Pu Differences Against CNES-CPP SWH

As a final step the SSH and Pu differences are analysed as a function of the SWH estimated by CNES-CPP, in order to identify possible dependencies of the errors on the SWH. Figure 22 (SSH difference vs SWH), and Figure 23 (Pu difference vs SWH) indicate the error tends to be a bit higher for the lower SWHs.

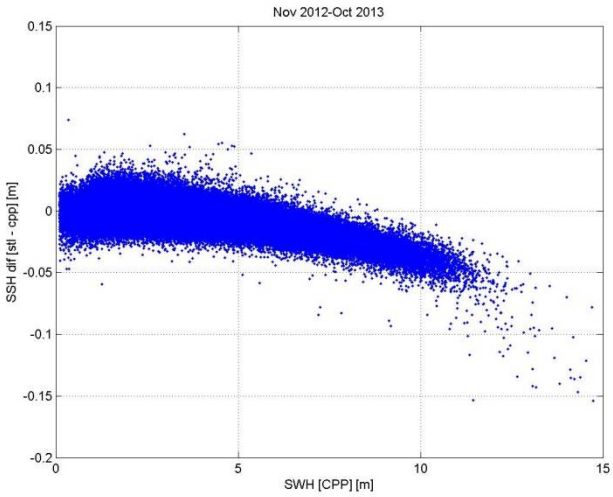

Figure 22- SSH error (SSH Starlab - SSH CNES-CPP) vs SWH CNES-CPP.

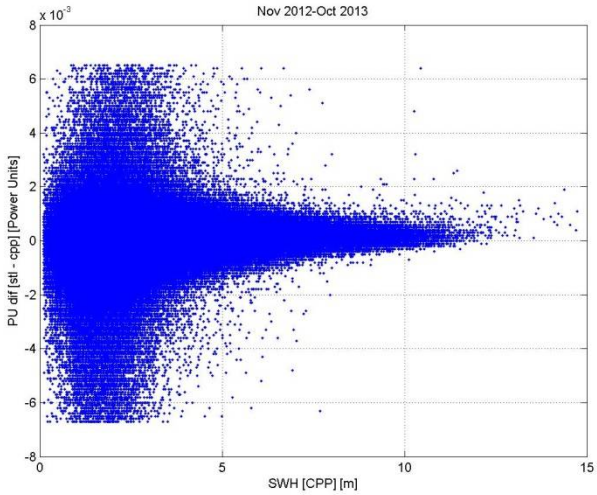

Figure 23- Pu error (Pu Starlab - Pu CNES-CPP) vs SWH CNES-CPP.

4.7 Error Analysis: Summary

Table 3 summarizes the main SSH, SWH, and Pu errors (bias + the std of the error mean, and std) obtained for the new retracker with respect to the CPP retracker. It is important to note that those results have been obtained after analysing filtered data collected during one year of observations.

Table 3- Error bias, and std, obtained for the retrieved parameters.

	SSH		SWH		Pu	
	Bias	**Std**	**Bias**	**Std**	**Bias**	**Std**
Error	**0.0039±5.52e-6**$\left(\sim\frac{0.0070}{\sqrt{1589461}}\right)$	**0.0070**	**-0.011±5.33e-7**$\left(\sim\frac{0.119}{\sqrt{1589461}}\right)$	**0.119**	**1.04e-4±5.22e-7**$\left(\sim\frac{6.59e-4}{\sqrt{1589461}}\right)$	**6.59e-4**

In general terms, the parameters retrieved with the optimised SAMOSA retracker show good agreement with those retrieved by the CPP retracker, with a correlation higher than 99%. The analysis has also shown that errors in the retrieved parameters are higher for lower SWHs. This trend should be further investigated.

5 Conclusions

5.1 Summary of Main Findings

An improved version of the thermal noise estimation for the SAMOSA retracker was developed in the framework of the WP3000 of CP4O CCN1. The approach is based on an empirical method, which estimated the beginning of the leading edge and then added a fixed extra margin. The main objective of the work presented here was to find the optimum margin and the number of lags that should be applied in the estimation of the thermal noise.

Different margins and number of lags have been tested using Level-1b CPP products, and the SSH, SWH, and Pu values from CPP products have been compared against those obtained by the modified SAMOSA retracker. The best results were obtained by using a margin of 16 lags and a window length of 2-3 lags. The equations adopted to estimate the thermal noise are the following.

leading_edge_span = 2*(waveform_peak_pos – half_power_pos),

leading_edge_starting_pos=waveform_peak_pos-leading _edge_span,

noise_calculation_position=leading_edge_starting_pos-(16),

noise_floor = mean(waveform[noise_calculation_position– 1: noise_calculation_position +1]),

In order to perform a statistically representative comparison, one year of CryoSat-2 data was used. The main results show a consistent equivalence between the 20 Hz products obtained from the modified SAMOSA and from the CPP retracker. An error bias of about 3.7 mm, with a standard deviation of 1 mm was obtained for the estimation of the SSH. The equivalent error bias for SWH was close to 1 cm, and quite low (0.0001 units) for the Pu. Major discrepancies between the SAMOSA and CNES retrackers were found in low SWH conditions. Validation against an independent dataset from buoys has been performed in RD.11.

5.2 Recommendations

- Further analysis to establish the cause of the large percentage of bad records (Figure 15).

- Further characterisation of the errors at low SWH.
- A comparison with results from the typical SAMOSA re-tracker would confirm that a real improvement has been achieved.

6 References

RD.1 CryoSat Plus for Oceans, Technical Proposal, SatOC, DTU Space,isardSAT, NOC, Noveltis, STARLAB, TU Delft, University of Porto and CLS,Response to ESA ITT AO/1-6827/11/I-NB, November 2011.

RD.2 CryoSat Plus for Oceans - Scientific Requirements Consolidation (D1.1),STARLAB, NOC, CLS, DTU Space, SatOC, ESA Project Report, March 2013.

RD.3 CryoSat Plus for Oceans – Preliminary Analysis Review (D2.1), TU Delft,CLS, DTU Space, isardSAT, NOC, Noveltis, SatOC, STARLAB, University of Porto, ESA Project Report, May 2013.

RD.4 CryoSat Plus for Oceans – Data Set User Manual (D3.2), isardSAT, SatOC,CLS, DTU Space, NOC, Noveltis, STARLAB, TU Delft, University of Porto,ESA Project Report, May 2013.

RD.5 CryoSat Plus for Oceans, Project Plan v3.1, SatOC, May 2013.

RD.6 CryoSat Plus for Oceans, Financial, Administrative and ManagementProposal, SatOC, DTU Space, isardSAT, NOC, Noveltis, STARLAB, TU Delft,University of Porto and CLS, Response to ESA ITT AO/1-6827/11/I-NB,November 2011.

RD.7 CryoSat Plus for Oceans – Product Validation Report-Open Ocean (D4.2), isardSAT, SatOC,CLS, DTU Space, NOC, Noveltis, STARLAB, TU Delft, University of Porto,ESA Project Report, July 2014.

RD.8 Ray.C, and Martin-Puig.C, SAMOSA models trade-off technical note. D1 SAMOSA-3 project, WP2100, 2012.

RD.9 CryoSat Plus for Oceans – Product Validation Report : SAR Altimetry over the Open Ocean and Coastal Zone, C. Gommenginger, P Cipollini, H. Snaith ,ESA Project Report, June 2014.

RD.10CryoSat Plus for Oceans – Algorithm Theoretical Basis Documentof the CPP SAR numerical retrcaker for oceans, F Boy, T. Moreau,ESA Project Report, June 2013.

RD.11 CryoSat Plus 4 Oceans – SAMOSA SAR retracker improvements. Assessment of Evaluation Data Set, M. Passaro and D. Cotton, ESA Project Report, 2016.

APPENDIX A

DATA OUTPUT

From each L1b file, three output files have been generated.

[INPUT_FILENAME].RES1.dat

L2 data product generated by Starlab. Content:

- SOW.
- Latitude.
- Longitude.
- Altitude.
- Altitude rate.
- Range.
- Estimated SSH.
- Estimated SWH.
- Estimated Pu.
- GOF (Goodness of Fit) computed as $\sqrt{mean(Waveform_{sim} - Waveform_{real})^2}$

[INPUT_FILENAME].RES2.dat

CNES-CPP L2 data product. Content:

- SOW.
- Latitude.
- Longitude.
- Altitude.
- Altitude rate.
- Range.
- Estimated SSH.
- Estimated SWH.
- Estimated Pu.

[INPUT_FILENAME].RES3.dat

Contains the main SSH and SWH bias and std error.

- $Mean\left(SSH_{starlab} - SSH_{cpp}\right)$.
- $Std\left(SSH_{starlab} - SSH_{cpp}\right)$
- $Mean\left(SWH_{starlab} - SWH_{cpp}\right)$
- $Std\left(SWH_{starlab} - SWH_{cpp}\right)$

APPENDIX B

THRESHOLD DEFINITION

During the processing of the L1b data, we identified cases where the retracker was not working properly. In those cases, the waveforms presented high amplitude values, and a sharply peaked shape. Figure 24 gives an example. On the left all the waveforms included in the file'CS_OPER_SIR1TKSA0__20130101T223228_20130101T223502_0001.DBL.DOP10.ES.DOP1B.RESDOP20.RES' have been plotted sequentially (the x axis represents the different acquisitions (waveforms), the y axis represents the gates of each wavefom,whereas the amplitude value is encoded in the colour). On the right all the 3000 waveforms included in CS_OPER_SIR1TKSA0__20130101T223228_20130101T223502_0001.DBL.DOP10.RES.DOP1B.RESDOP20.RES have been represented over the same plot. These waveforms are sharply peaked (similar to land echoes), not having the typical shape of a waveform over ocean. Additionally, the amplitudes are quite high. Compared to the typical case (see Figure 25), they are quite different.

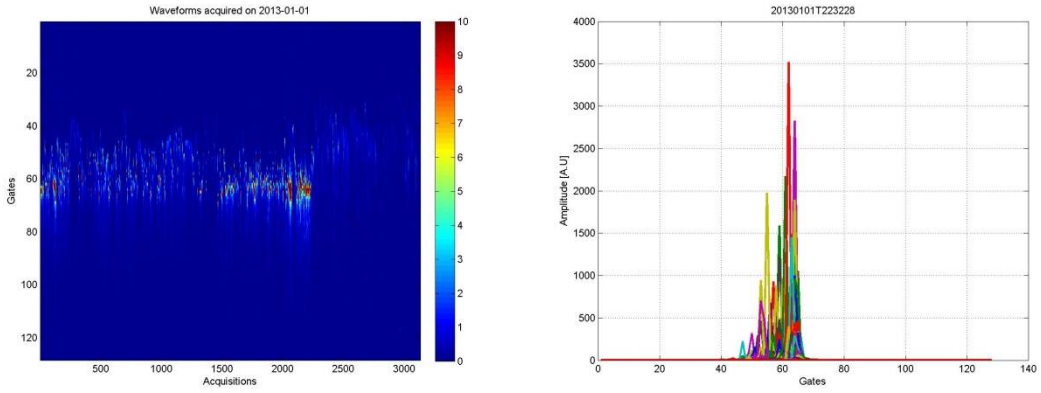

Figure 24- (left) Waveforms acquired on 2013-01-01 (from 22:32:28 to 22:35:02) plotted sequentially, (right) all the waveforms over the same plot.

Figure 25 shows the waveforms acquired on 2013-01-05, at 04:01:35. Here the amplitudes are much lower (below 2), and the shape follows the one of a typical waveform acquired over the ocean.

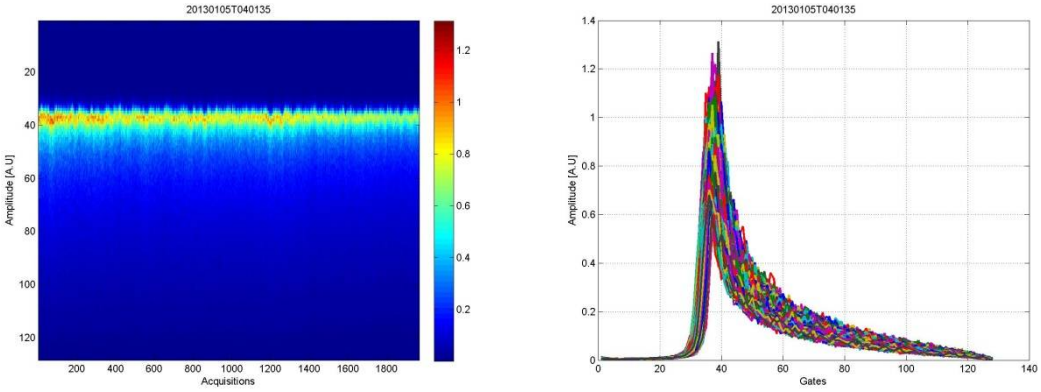

Figure 25- (left) Waveforms acquired on 2013-01-05 (at 04:01:35) plotted sequentially, (right) all the Waveforms over the same plot.

Waveforms like the ones shown in Figure 24 have been filtered using an amplitude threshold. The amplitude threshold has been defined based on the minimum amplitude of the waveforms contaminated. By using different files like CS_OPER_SIR1TKSA0__20130101T223228_20130101T223502_0001.DBL.DOP10.RES.DOP1B.RESDOP20.RES, it has been identified that when the amplitude is higher than 10, waveforms tend to be like the ones plotted in Figure 26. In that case, the file is discarded.

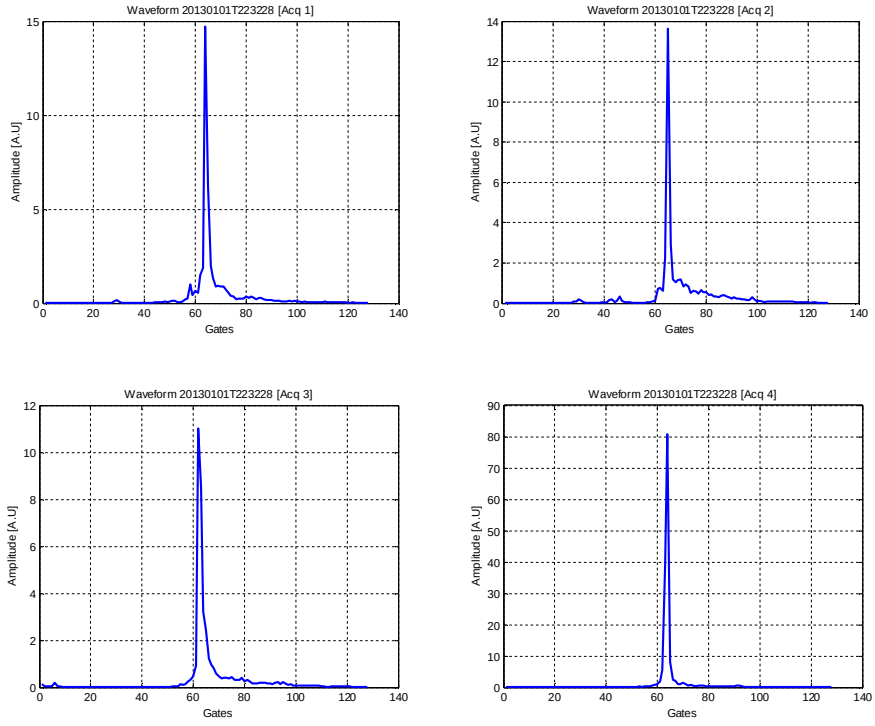

Figure 26- Four individual waveforms contained in the file CS_OPER_SIR1TKSA0__20130101T223228 _20130101T223502_0001.DBL.DOP10.RES.DOP1B.RESDOP20.RES.

EXAMPLE OF WRONG DATA AFTER FILTERING

Below we present examples of waveforms (from January 2013) discarded after filtering. The left panels show the waveforms plotted sequentially (the x axis represents the different acquisitions (waveforms), whereas the y axis represents the gates of each waveform. The right panels show the different waveforms over the same plot.

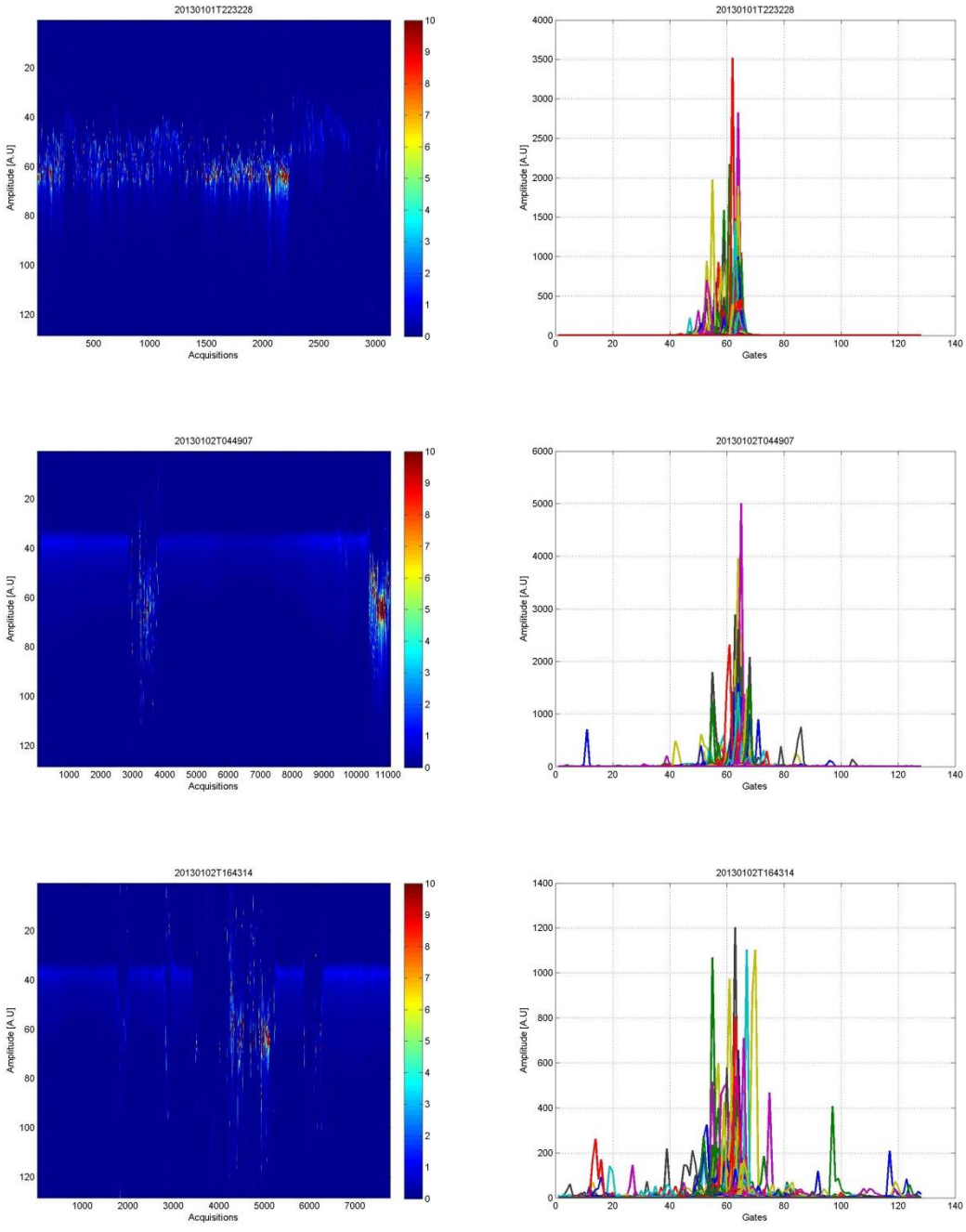

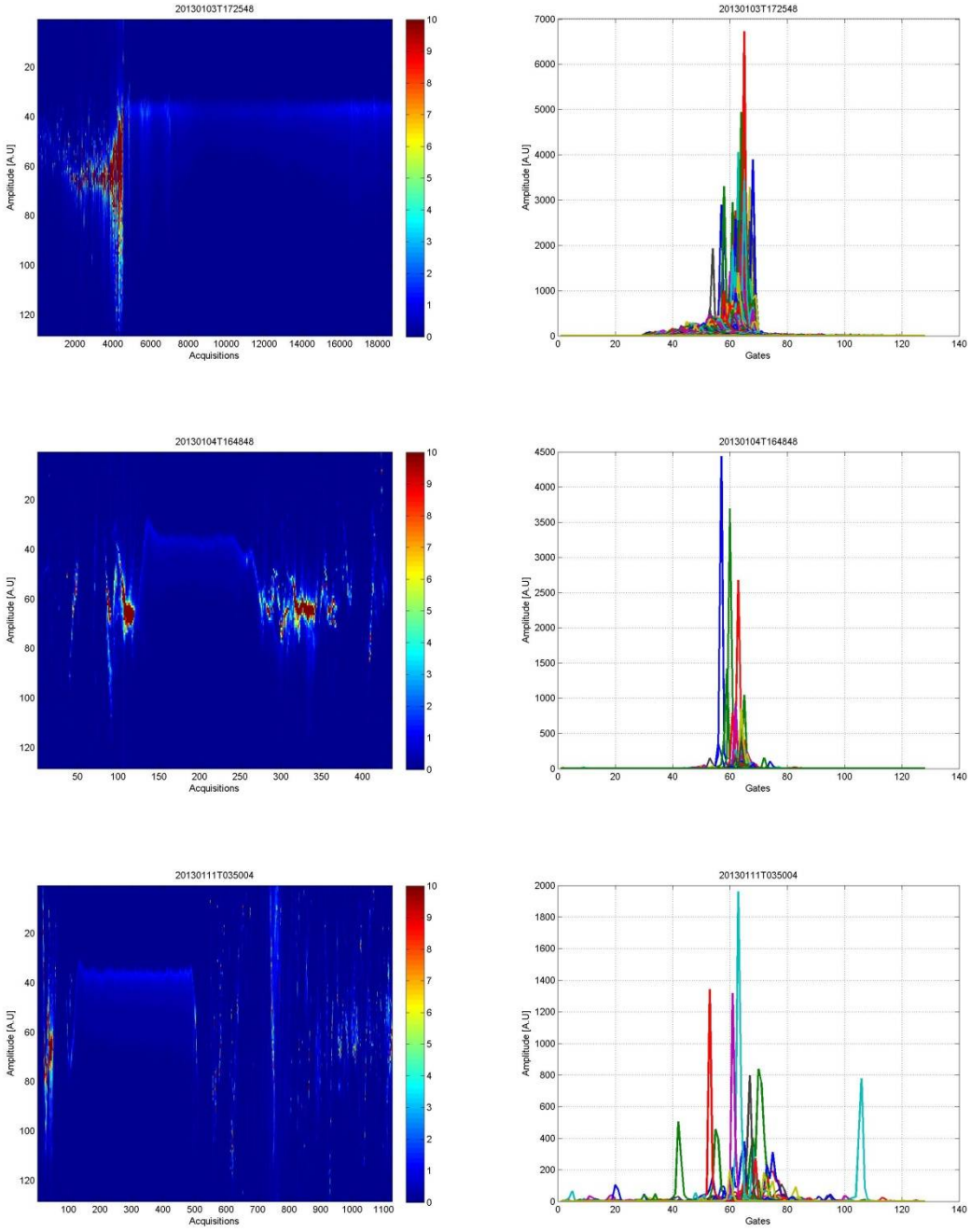

Figure 27- Example of waveforms discarded after filtering, corresponding respectively to: 2013-01-01 at 22:32:28, 2013-01-02 at 04:49:07, 2013-01-02 at 16:43:14, 2013-01-03 at 17:25:48, 2013-01-04 at 16:48:48, and 2013-01-11 at 03:50:04.

List of Acronyms

ATBD	Algorithm Theoretical Basis Document
BRF	Burst repetition Frequency
CCN	Contract Change Notice
CLS	Collecte Localisation Satellites
CNES	Centre National d'ÉtudesSpatiales
CP4O	CryoSat Plus 4 Oceans
CPP	CryoSat Processing Prototype
CRYMPS	CryoSat-2 Mission Performance Simulator
CryoSat, C2	ESA mission to study the cryosphere. It includes a SARin altimeter.
ESA	European Space Agency
ESRIN	ESA Centre forEarth Observation / ESA Space Research Institute
FBR	Full Bit Rate
LMS	Least Mean Squares
LRM	Low Resolution Mode
NOAA	National Oceanic and Atmospheric Administration
NOC	National Oceanography Centre
PRF	Pulse Repetition Frequency
Pu	Received Power
RDSAR	Reduced SAR
SAMOSA	Analytical SAR altimeter ocean echo model developed in SAMOSA project
SAR	Synthetic Aperture Radar
SatOC	Satellite Oceanographic Consultants
Sigma-o	Surface radar backscatter at nominal incidence
SIRAL	Synthetic aperture Interferometric Radar ALtimeter
SNR	Signal-to-Noise Ratio
STD	Standard Deviation
STSE	ESA's Support To Science Element programme
SSB	Sea Surface Bias
SSH	Sea Surface Height
SWH	Significant Wave Height
TN	Thermal Noise
TU Delft	Delft University of Technology